Many Light Higgs Bosons in the NMSSM

Radovan Dermíšek[1,*] and John F. Gunion[2,†]

[1] *Physics Department, Indiana University, Bloomington, IN 47405*
[2] *Department of Physics, University of California at Davis, Davis, CA 95616*

(Dated: November 21, 2008)

The next-to-minimal supersymmetric model with a light doublet-like CP-odd Higgs boson and small $\tan\beta$ can satisfy all experimental limits on Higgs bosons even with light superpartners. In these scenarios, the two lightest CP-even Higgs bosons, h_1 and h_2, and the charged Higgs boson, h^+, can all be light enough to be produced at LEP and yet have decays that have not been looked for or are poorly constrained by existing collider experiments. The channel $h_1 \to a_1 a_1$ with $a_1 \to \tau^+\tau^-$ or $2j$ is still awaiting LEP constraints for $m_{h_1} > 86$ GeV or 82 GeV, respectively. LEP data may also contain $e^+e^- \to h_2 a_1$ events where $h_2 \to Z a_1$ is the dominant decay, a channel that was never examined. Decays of the charged Higgs bosons are often dominated by $H^\pm \to W^{\pm(\star)} a_1$ with $a_1 \to gg, c\bar{c}, \tau^+\tau^-$. This is a channel that has so far been ignored in the search for $t \to h^+ b$ decays at the Tevatron. A specialized analysis might reveal a signal. The light a_1 might be within the reach of B factories via $\Upsilon \to \gamma a_1$ decays. We study typical mass ranges and branching ratios of Higgs bosons in this scenario and compare these scenarios where the a_1 has a large doublet component to the more general scenarios with arbitrary singlet component for the a_1.

I. INTRODUCTION

Discovery of Higgs bosons and exploration of their properties is the key to understanding electroweak symmetry breaking and a major step in uncovering the ultimate theory of particle physics. The Higgs boson is the last missing piece of the standard model (SM). In theories beyond the SM the Higgs sector is typically more complicated, *e.g.* in the minimal supersymmetric model (MSSM) there are two Higgs doublets which lead to five Higgs bosons in the spectrum: light and heavy CP-even Higgses, h and H, a CP-odd Higgs, A, and a pair of charged Higgs bosons, $H^\pm$. In the next-to-minimal supersymmetric model (NMSSM) which contains an additional singlet superfield with complex component scalar field there are three CP-even Higgses, $h_{1,2,3}$, two CP-odd Higgses, $a_{1,2}$ and a pair of charged Higgs bosons; and there are many simple models with an even more complicated Higgs sector.

Since searches for Higgs bosons rely on detection of their decay products, it is crucial to understand the way the Higgs bosons decay. Although it is usually the case that one of the Higgs bosons has couplings to the W, Z bosons and to fermions that are close to those of the SM Higgs, it is not necessarily true that such a Higgs decays in the way the SM Higgs does [1]. A significant model dependence of decay modes applies to other Higgses as well.

It has been recently argued that supersymmetric models in the region of parameter space for which $\tan\beta$ is small and, in addition, there is a light doublet-like CP-odd Higgs predict that all the Higgses resulting from the two Higgs doublets (h, H, A and $H^\pm$) could have been produced already at LEP or the Tevatron, but would have escaped detection because the decay modes have either not been searched for (or the searches have been incomplete) or are ones to which the experiments are not sensitive. Although this scenario is ruled out in the MSSM, it is only marginally disallowed for $m_A < 2m_b$ and $\tan\beta \lesssim 2.5$ and thus can possibly be viable in simple extensions of the MSSM [2]. The reason is that for $m_A \ll m_W$ and $\tan\beta \simeq 1$ the light CP-even Higgs boson becomes SM-like, and although it is massless at the tree level, its mass will receive a contribution from superpartners and the tree level relation between the light CP-even and CP-odd Higgses, $m_h < m_A$, is dramatically changed by SUSY corrections. Even for modest superpartner masses the light CP-even Higgs boson will be heavier than $2m_A$. In particular, for superpartner masses between 300 GeV and 1 TeV and $\tan\beta \simeq 1$, one finds $m_h \simeq 40 - 60$ GeV and the $h \to AA$ decay mode is open and generically dominant.

Since the h has SM-like WW, ZZ couplings, $e^+e^- \to hA$ is highly suppressed and the limits from the Z width measurements can be easily satisfied even for $m_h + m_A < m_Z$. On the other hand, the $e^+e^- \to Zh$ cross section would be maximal. However, for $\tan\beta \sim 1$ and $m_A < 2m_b$ the decay width of the A is shared between $\tau^+\tau^-$, $c\bar{c}$ and gg final states and thus the (dominant) $h \to AA$ decays are spread over many different final states: 4τ, $2\tau 2g$, $4g$, $4c$, $2g2c$, $2\tau 2c$ and $b\bar{b}$, the latter being greatly suppressed relative to the SM expectation due to the presence of the $h \to AA$ decays. As a consequence, the LEP limits in each channel separately are very substantially weakened. Of course, the decay mode independent limit requires a Higgs with SM-like ZZ coupling to be above 82 GeV [3]. It is this fact that rules out this scenario in the MSSM, since there m_h cannot be pushed above 82 GeV by radiative corrections.

The rest of the Higgs spectrum is basically not constrained at all in this scenario. The heavy CP-even and

*dermisek@indiana.edu
†gunion@physics.ucdavis.edu

the CP-odd Higgses could have been produced at LEP in $e^+e^- \to HA$ but they would have escaped detection because H dominantly decays to ZA - a mode that has not been searched for. Additional constraints are discussed in detail in Ref. [2]. The charged Higgs is also very little constrained and up to $\sim 40\%$ of top quarks produced at the Tevatron could have decayed into charged Higgs and the b quark since the dominant decay mode for the charged Higgs $H^\pm \to W^{\pm(\star)}A$ with $A \to c\bar{c}$, gg or $\tau^+\tau^-$ would not have been separated from the the generic top sample [1]. In addition, pair production of a charged Higgs boson with the properties emerging in this scenario and mass close to the mass of the W boson could explain the 2.8σ deviation from lepton universality in W decays measured at LEP [4] as discussed in [5].

The mass of the light CP-even Higgs is the only problematic part in this scenario. There are however various ways to increase the mass of the SM-like Higgs boson in extensions of the MSSM. A simple possibility is to consider singlet extensions of the MSSM containing a $\lambda \widehat{S}\widehat{H}_u\widehat{H}_d$ term in the superpotential. It is known that this term itself contributes $\lambda^2 v^2 \sin^2 2\beta$, where $v = 174$ GeV, to the mass squared of the CP-even Higgs [6] and thus can easily push the Higgs mass above the decay-mode independent limit of 82 GeV. Note that this contribution is maximized for $\tan\beta \simeq 1$. In addition, it need not be the case that the light CP-even Higgs has full strength ZZ coupling, in which case the model-independent limit on m_h is reduced, while at the same time the H which carries the rest of the ZZ coupling can have mass above the LEP kinematic reach and/or decay to modes for which the LEP limit of 114 GeV does not apply. Thus, it is not surprising that in the NMSSM it is possible to find scenarios in which the lightest CP-odd Higgs has mass below $2m_b$ and the two lightest CP-even Higgs bosons and the charged Higgs would all have been produced at LEP and yet escaped detection.

In this paper we study NMSSM scenarios with a light CP-odd Higgs boson and small $\tan\beta$. We will in particular examine the subset of these scenarios in which the light CP-odd Higgs boson is mainly doublet-like (a_1-doublet-like scenarios) and will find that they have many features in common with the MSSM scenarios discussed above, except that they are not ruled out by Higgs searches — they are phenomenologically viable even with very light superpartners. For the subset of the a_1-doublet-like scenarios in which the h_1 has nearly SM-like couplings, the h_1 can be as light as 82 GeV (the decay-mode independent limit) by virtue of dominant decays $h_1 \to a_1 a_1 \to 2\tau 2c, 4\tau, 4c$, *etc.*. There are also scenarios for which the h_1 has reduced coupling to ZZ, $g^2_{ZZh_1}/g^2_{ZZh_{\rm SM}} \simeq 0.5$. [2] In these latter cases, the CP-even Higgs boson can have m_{h_1} as low as ~ 55 GeV. All these scenarios are similar to the scenario with a light singlet-like CP-odd Higgs in the NMSSM [7, 8, 9, 10, 11] in that it is the unexpected Higgs decays that allow one or more light Higgs bosons to have escaped LEP detection. The important difference is that the scenario discussed in Refs. [7, 8, 9, 10, 11] is the usual decoupled scenario as far as the two Higgs doublet part of the Higgs spectrum is concerned (the CP-odd Higgs, the heavy CP-even Higgs and the charged Higgs are heavy and approximately degenerate) and the light CP-odd Higgs is supplied by the additional singlet. In contrast, in the a_1-doublet-like low-$\tan\beta$ scenarios, the CP-even and CP-odd Higgses coming from the additional singlet are typically heavy and do not drastically alter the two Higgs doublet part of the Higgs sector. The latter then looks like the Higgs sector of the MSSM with somewhat modified mass relations.

II. LIGHT DOUBLET-LIKE a_1 IN THE NMSSM

As already mentioned the scenario with a light doublet-like CP-odd Higgs and small $\tan\beta$ is phenomenologically viable in the simplest extension of the MSSM, the next-to-minimal supersymmetric model which adds only one singlet chiral superfield, $\widehat{S}$. The very attractive nature of the NMSSM extension of the MSSM on general grounds has been discussed for many years [14]; in particular, it avoids the need for the μ parameter of the MSSM superpotential term $\mu\widehat{H}_u\widehat{H}_d$. The NMSSM particle content differs from the MSSM by the addition of one CP-even and one CP-odd state in the neutral Higgs sector (assuming CP conservation), and one additional neutralino. We will follow the conventions of [15]. Apart from the usual quark and lepton Yukawa couplings, the scale invariant superpotential is

$$\lambda\ \widehat{S}\widehat{H}_u\widehat{H}_d + \frac{\kappa}{3}\ \widehat{S}^3 \qquad (1)$$

depending on two dimensionless couplings λ, κ beyond the MSSM. [Hatted (unhatted) capital letters denote superfields (scalar superfield components).] An effective μ term arises from the first term of Eq. (1) when the scalar component of $\widehat{S}$ acquires a vacuum expectation value, $s \equiv \langle\widehat{S}\rangle$, yielding

$$\mu_{\rm eff} = \lambda s\,. \qquad (2)$$

The trilinear soft terms associated with the superpotential terms in Eq. (1) are

$$\lambda A_\lambda S H_u H_d + \frac{\kappa}{3} A_\kappa S^3\,. \qquad (3)$$

[1] We thank Ricardo Eusebi (CDF) for a detailed discussion of the CDF and D0 analyses.

[2] In general, in singlet extensions it is possible to alter the couplings of the Higgses to Z and W through mixing, see e.g. Refs. [12, 13] or to provide new Higgs decay modes [1].

The final input parameter is

$$\tan\beta = h_u/h_d\,, \tag{4}$$

where $h_u \equiv \langle H_u\rangle$, $h_d \equiv \langle H_d\rangle$. The vevs h_u, h_d and s, along with m_Z, can be viewed as determining the three SUSY breaking masses squared for H_u, H_d and S (denoted $m^2_{H_u}$, $m^2_{H_d}$ and m^2_S) through the three minimization equations of the scalar potential. Thus, as compared to the three independent parameters needed in the MSSM context (often chosen as μ, $\tan\beta$ and M_A), the Higgs sector of the NMSSM is described by the six parameters

$$\lambda\ ,\ \kappa\ ,\ A_\lambda\ ,\ A_\kappa,\ \tan\beta\ ,\ \mu_{\rm eff}\ . \tag{5}$$

(We employ a convention in which all parameters are evaluated at scale m_Z unless otherwise stated.) We will choose sign conventions for the fields such that λ and $\tan\beta$ are positive, while κ, A_λ, A_κ and $\mu_{\rm eff}$ should be allowed to have either sign. In addition, values must be input for the gaugino masses ($M_{1,2,3}$) and for the soft terms related to the (third generation) squarks and sleptons (m^2_Q, m^2_U, m^2_D, m^2_L, m^2_E, A_t, A_b and A_τ) that contribute to the radiative corrections in the Higgs sector and to the Higgs decay widths. For small $\tan\beta$, the soft parameters which play the most prominent role are m^2_Q, m^2_U and A_t.

A complete survey of the parameter space is difficult. To present results in a manageable way, we fix μ and $\tan\beta$ together with all soft SUSY breaking masses and scan over trilinear and soft-trilinear couplings. We will plot results in various two-dimensional planes. The input parameters of Eq. (3) are scanned over the following regions with fixed steps: $\lambda \in (0.001, 0.6)$ using 60 steps of size 0.01; $\kappa \in (-0.6, 0.6)$ using 120 steps of size 0.01, with some refined scans for $\kappa \in (-0.06, 0.06)$ using 120 steps of size 0.001; $A_\lambda \in (-600\,{\rm GeV}, 600\,{\rm GeV})$ using 200 steps of size 6 GeV; and finally $A_\kappa \in (-600\,{\rm GeV}, 600\,{\rm GeV})$ using 200 steps of size 6 GeV, with refined scans for this same range with 1000 steps of size 1.2 GeV. Varying the fixed soft SUSY breaking masses leads to smaller changes than does varying $\tan\beta$. Thus, we will consider only a few choices of soft SUSY breaking masses and will focus on the important changes that occur as $\tan\beta$ is changed.

All scans are performed in the context of NMHDECAY. NMHDECAY checks a long list of experimental constraints, especially those coming from LEP data. It also checks various theoretical constraints on the model incorporated, such as requiring that the vacuum be a true vacuum. NMHDECAY also issues a warning if any of the couplings, λ, κ, h_t or h_b become non perturbative (h_t and h_b are the Yukawa couplings) after evolution to the GUT scale. We will consider scenarios in which these become non-perturbative as well as scenarios in which they remain perturbative. Aside from this, all plotted points are consistent with all the NMHDECAY constraints.

As stated in the introduction, we wish to focus on cases for which $m_{a_1} < 10$ GeV. Such scenarios have the most unusual features. In this mass region, it is important to incorporate the constraints arising from recently improved limits on $B(\Upsilon \to \gamma a_1)$ with $a_1 \to \tau\tau$ from CLEO-III [20] as well as old CUSB-II limits [21] on $B(\Upsilon \to \gamma a_1)$ where a_1 is only assumed to be visible. These basically place an upper limit on the $b\overline{b}a_1$ coupling defined by

$$\mathcal{L}_{a_1 b\overline{b}} \equiv iC_{a_1 b\overline{b}}\frac{ig_2 m_b}{2m_W}\overline{b}\gamma_5 b a_1 \tag{6}$$

in the region $m_{a_1} < m_\Upsilon$. Further constraints on this coupling were obtained at LEP by looking for $b\overline{b}a_1$ production with $a_1 \to \tau\tau$ and $a_1 \to b\overline{b}$ [22, 23]. The former channel is important in the $m_{a_1} < 10$ GeV that we focus on. The upper limits on $C_{a_1 b\overline{b}}$ using the above inputs are given in Fig. 1 of [24]. At any given $\tan\beta$, a limit $|C_{a_1 b\overline{b}}|^{\rm max}$ on $|C_{a_1 b\overline{b}}|$ converts to a limit on $|\cos\theta_A|$ using $C_{a_1 b\overline{b}} = \cos\theta_A \tan\beta$, *i.e.* $|\cos\theta_A| \le |C_{a_1 b\overline{b}}|^{\rm max}/\tan\beta$. The resulting values for $|\cos\theta_A|^{\rm max}$ appear in Fig. 3 of [24]. It also turns out that Tevatron limits on $pp \to a_1 \to \mu^+\mu^-$ provide some constraints on $C_{a_1 b\overline{b}}$ in the region from 8 GeV $< m_{a_1} <$ 9 GeV that are stronger than those from e^+e^- data [25]. These too are incorporated.

A final addendum to NMHDECAY is to include off-shell decays involving an a_1 and a gauge boson in the final state. In particular, $h^+ \to W^* a_1$ and $h_2 \to Z^* a_1$ virtual decays are of occasional importance in the small m_{a_1} region.

A. Results for $\tan\beta = 2$

A convenient reference scenario is the case of $\tan\beta = 2$ with $M_{SUSY} = 300$ GeV and $A_t = A_b = A_\tau = -300$ GeV. The plots for this case are Figs. 1 – 23. In our plots, the blue +'s are all points that satisfy the NMHDECAY constraints, while green diamonds are those which in addition have a light CP-odd Higgs which is doublet-like, $\cos^2\theta_A > 0.5$. The red crosses single out those points for which $m_{h_1} < 65$ GeV. Because of the limits on $|\cos\theta_A|$ discussed above, m_{a_1} values below about 7.5 GeV are disallowed for $\cos^2\theta_A > 0.5$, as are many points with $\cos^2\theta_A < 0.5$. This is illustrated in Fig. 1. The jagged shape of the boundary in the $m_{a_1} < 7.5$ GeV region for the $\cos^2\theta_A < 0.5$ points simply reflects the rather rapid variations in the limits from $B(\Upsilon \to \gamma a_1)$ decays.

The first plot, Fig. 2 shows the m_{h_1} masses that are obtained in our scan and the correlation with m_{a_1}. Higgs with $m_{h_1} < 114$ GeV are not excluded by LEP data. The reason is apparent from Figs. 3, 4 and 5. There, we plot $C^2_V(h_1) \equiv g^2_{ZZh_1}/g^2_{ZZh_{\rm SM}}$, $B(h_1 \to a_1 a_1)$ and $C^2_V(h_1)B(h_1 \to b\overline{b})$ vs. m_{h_1}. We see that the light h_1 escapes LEP constraints mainly because of large $B(h_1 \to a_1 a_1)$ (where $a_1 \to \tau^+\tau^-$ yields a 4τ final state that is weakly constrained by LEP data) although there are a significant number of points for which the a_1 is mainly singlet with small $C^2_V(h_1)$. The plot of Fig. 5 shows the

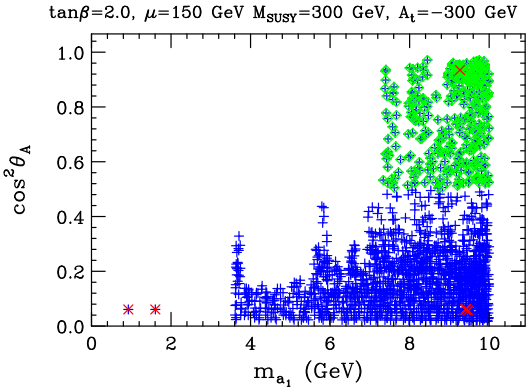

FIG. 1: $\cos^2\theta_A$ is plotted vs. m_{a_1} for the $\tan\beta = 2$, $m_{\rm SUSY} = 300$ GeV, $A = -300$ GeV scenario.

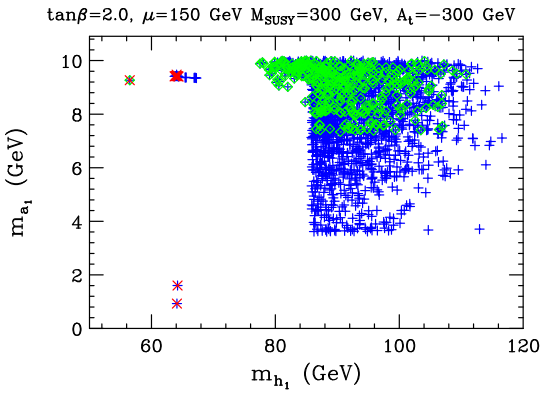

FIG. 2: m_{a_1} is plotted vs. m_{h_1} for the $\tan\beta = 2$, $m_{\rm SUSY} = 300$ GeV, $A = -300$ GeV scenario.

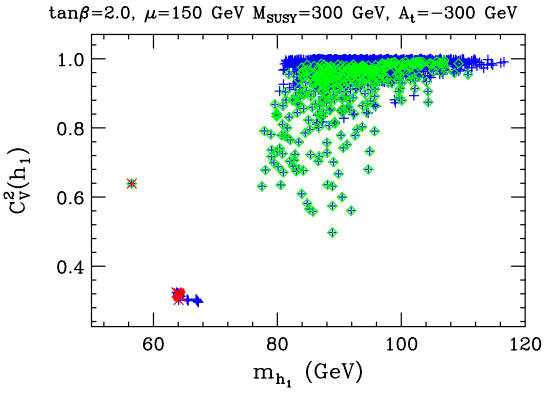

FIG. 3: $C_V^2(h_1)$ is plotted vs. m_{h_1} for the $\tan\beta = 2$, $m_{\rm SUSY} = 300$ GeV, $A = -300$ GeV scenario.

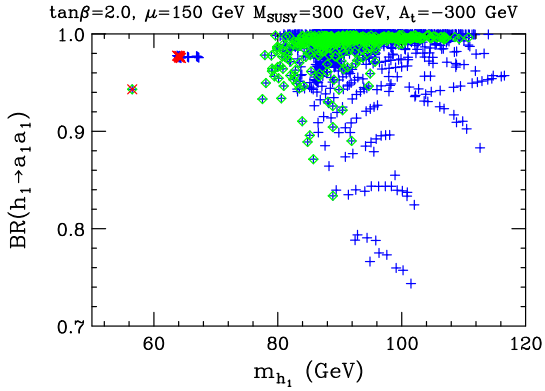

FIG. 4: $B(h_1 \to a_1 a_1)$ is plotted vs. m_{h_1} for the $\tan\beta = 2$, $m_{\rm SUSY} = 300$ GeV, $A = -300$ GeV scenario.

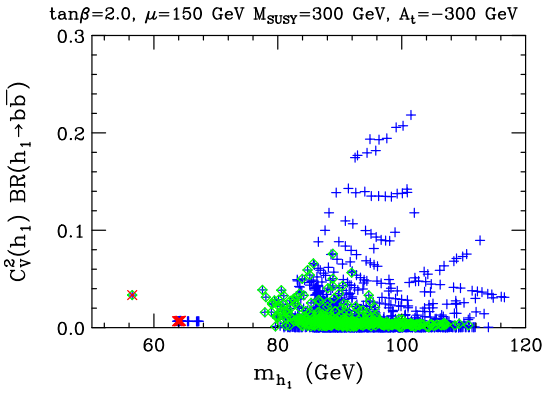

FIG. 5: $C_V^2(h_1)B(h_1 \to b\bar{b})$ is plotted vs. m_{h_1} for the $\tan\beta = 2$, $m_{\rm SUSY} = 300$ GeV, $A = -300$ GeV scenario.

net rate for $e^+e^- \to Zb\bar{b}$ relative to the SM prediction. We observe that away from the 90 GeV to 105 GeV window in $m_{h_1} = m_{b\bar{b}}$, in which there is an excess of LEP events relative to background, this net rate must be quite small. In the 90 GeV to 105 GeV window, the best fit to the experimental data corresponds to an an excess of order 0.1 times the expected SM rate is allowed. However, in this window, an excess as large as 0.2 times the SM rate is still allowed at 90% CL, as reflected in the plot. Note that it is mainly the points with $\cos^2\theta_A \lesssim 0.5$ that best explain the observed $0.1\times$ SM excess in this region.

The next interesting feature of these small m_{a_1}, small $\tan\beta$ scenarios is the very substantial probability that the h^+ will also be quite light. As shown in Fig. 6, this is particularly the case for parameters such that the a_1 is mainly doublet. For these a_1-doublet-like scenarios, we observe that there are cases for which m_{h_1} is well below 100 GeV while m_{h^+} is of order 100 GeV, and in the vast majority of these a_1-doublet-like scenarios $m_{h^+} < 170$ GeV so that the h^+ would have been produced in top decays. At the same time, as shown in Fig. 7, for the a_1-doublet-like scenarios m_{h_2} can also be of order 100 GeV, and in nearly all cases $m_{h_2} < 200$ GeV so that $e^+e^- \to Zh_2$ production events would be present in LEP data. In the case of $m_{h_2} \sim 100$ GeV it is the reduced $C_V^2(h_2)$ (Fig. 8) coupled with large $B(h_2 \to a_1 a_1)$ (Fig. 9) that makes LEP sensitivity in the $Zh_2 \to Zb\bar{b}$ channel small. Indeed, Fig. 10 shows that the h_2 contribution to the $Zh_2 \to Zb\bar{b}$ channel can only be significant for $m_{h_2} \sim 125$ GeV, well above the LEP kine-

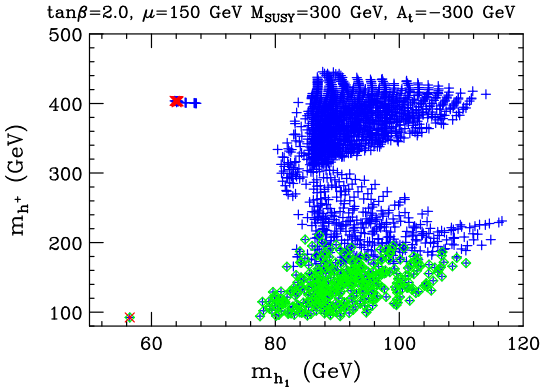

FIG. 6: m_{h^+} is plotted vs. m_{h_1} for the $\tan\beta = 2$, $m_{\rm SUSY} = 300$ GeV, $A = -300$ GeV scenario.

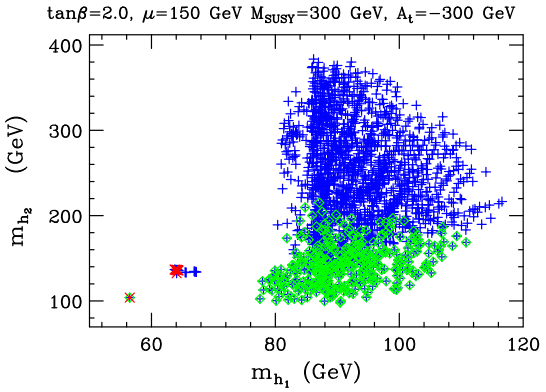

FIG. 7: m_{h_2} is plotted vs. m_{h_1} for the $\tan\beta = 2$, $m_{\rm SUSY} = 300$ GeV, $A = -300$ GeV scenario.

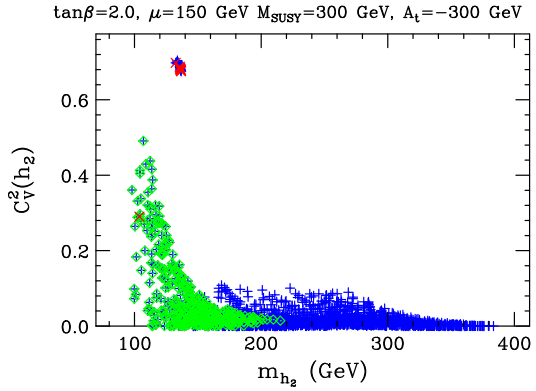

FIG. 8: $C_V^2(h_2)$ is plotted vs. m_{h_2} for the $\tan\beta = 2$, $m_{\rm SUSY} = 300$ GeV, $A = -300$ GeV scenario.

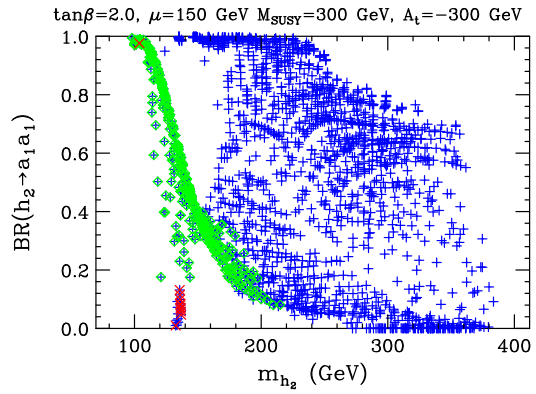

FIG. 9: $B(h_2 \to a_1 a_1)$ is plotted vs. m_{h_2} for the $\tan\beta = 2$, $m_{\rm SUSY} = 300$ GeV, $A = -300$ GeV scenario.

matic reach. (However, as we shall see, this conclusion does not apply to all choices of $\tan\beta$ and soft-SUSY-breaking parameters.) For these same scenarios with large $\cos^2\theta_A$, the a_1 and h_2 both have substantial doublet component, and the $Z \to h_2 a_1$ rate at LEP would also have been significant. For m_{h_2} near 100 GeV, the $h_2 a_1$ final states would have escaped LEP detection because of large $B(h_2 \to a_1 a_1)$. For larger m_{h_2} up near 200 GeV, $B(h_2 \to Z a_1)$ would have been large, see Fig. 11, and LEP did not analyze their data in such a way as to be sensitive to $h_2 a_1 \to Z a_1 a_1$ final states, especially given that a_1 decays to either two taus or two jets.

Turning to the charged Higgs boson, most LEP searches for the h^+ were based on the dominant $e^+e^- \to h^+h^-$ production mechanism assuming that $h^+ \to \tau^+\nu_\tau$ and $h^+ \to c\overline{s}$ were the only two decay modes. However, Fig. 12 shows that $h^+ \to W^{+(*)} a_1$ is dominant for the a_1-doublet-like scenarios. Limits on m_{h^+} weaken as $B(h^+ \to \tau^+\nu_\tau)$ declines — if $B(h^+ \to \tau^+\nu_\tau) \sim 1, 0.5, 0$ the limits are roughly $m_{h^+} > 90, 80, 80$ GeV, respectively [26]. DELPHI considered the possibility of $h^+ \to W^{+(*)} a$ assuming $a \to b\overline{b}$ is dominant [27]. However, their limits on m_{h^+} do not apply to the case of $m_a < 2m_b$ of interest here.

Overall, we have the remarkable result that for the chosen $\tan\beta = 2$ and $m_{\rm SUSY} = 300$ GeV, $A = -300$ GeV parameters there are a large number of model points (the a_1-doublet-like points) for which the h_1 and $h^\pm$ have mass at or below 100 GeV and the h_2 has mass in the range $100 - 190$ GeV. All would have been copiously produced

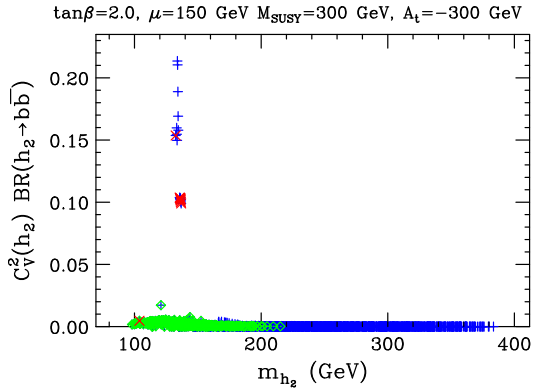

FIG. 10: $C_V^2(h_2) B(h_2 \to b\overline{b})$ is plotted vs. m_{h_2} for the $\tan\beta = 2$, $m_{\rm SUSY} = 300$ GeV, $A = -300$ GeV scenario.

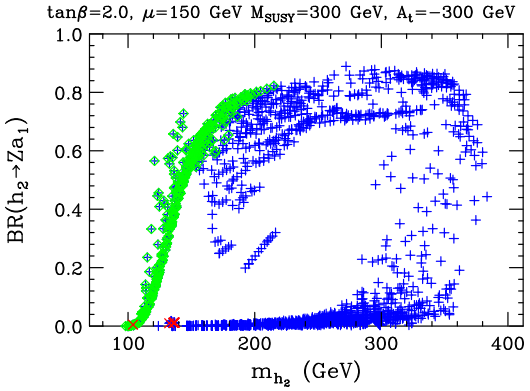

FIG. 11: $B(h_2 \to Z a_1)$ is plotted vs. m_{h_2} for the $\tan\beta = 2$, $m_{\rm SUSY} = 300$ GeV, $A = -300$ GeV scenario.

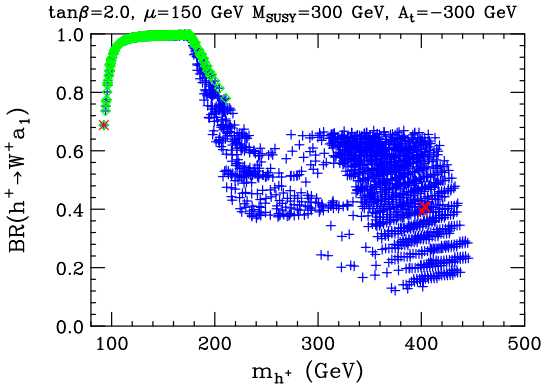

FIG. 12: $B(h^+ \to W^{+(\star)} a_1)$ is plotted vs. m_{h^+} for the $\tan\beta = 2$, $m_{\rm SUSY} = 300$ GeV, $A = -300$ GeV scenario.

at LEP, and yet all would have escaped LEP detection.

The primary sensitivity of the Tevatron to the a_1-doublet-like scenarios with a light h^+ is through searches for $t\bar{t}$ production with one t decaying via $t \to h^+ \bar{b}$ [28, 29, 30]. The recent preliminary Tevatron analyses [29, 30] set limits on the $B(t \to h^+ b) B(h^+ \to \tau^+ \nu_\tau)$ as a function of m_{h^+}. Fitting simultaneously the branching ratio product and $\sigma(p\bar{p} \to t\bar{t})$, the limit for $m_{h^+} = 80$ GeV is $B(t \to h^+ b) B(h^+ \to \tau^+ \nu_\tau) < 0.12$. In the present scenario, all these searches would have suppressed sensitivity for the cases where $m_{h^+} \sim 100$ GeV. The reason is that $h^+ \to W^{+(\star)} a_1$ always has branching ratio > 0.5, and the a_1 decays primarily to $\tau^+\tau^-$ for $m_{a_1} > 2m_\tau$ and to various lighter final states if $m_{a_1} < 2m_\tau$. $B(h^+ \to W^{+(\star)} a_1)$ is shown in Fig. 12. From Fig. 13, we see that $B(h^+ \to \tau^+ \nu_\tau) \sim 1 - B(h^+ \to W^{+(\star)} a_1)$ for $m_{h^+} < m_t + m_b$.

Of course, $B(t \to h^+ \bar{b})$ is $\tan\beta$ dependent. For $\tan\beta = 1.2, 1.7, 2$ it is of order $0.3, 0.173, 0.126$ for $m_{h^+} \sim 90$ GeV. For $m_{h^+} > m_t + m_b$ one finds that $h^+ \to t\bar{b}$ is the dominant decay. At $\tan\beta = 2$, $B(h^+ \to W^{+(\star)} a_1)$ can be of order 0.5 out to relatively large m_{h^+}. LHC search strategies sensitive to all these unusual scenarios need to be developed. Some discussion of the possibilities appears in Ref. [31].

Given the fact that the a_1 appears in so many decays, it is useful to review its branching ratios. In NMHDECAY, these are computed using partonic final states and masses. This implies a few inaccuracies. In particular, $a_1 \to s\bar{s}$ is non-zero even when $m_{a_1} < 2m_K$ since NMHDECAY employs $m_s = 0.19$ GeV. The a_1 branching ratios appear in Figs. 14, 15, 16 and 17. As expected, if $m_{a_1} < 2m_b$ but well above $2m_\tau$ (as is the case for all a_1-doublet-like scenarios), $a_1 \to \tau^+\tau^-$ is the dominant decay, with the remainder being in the $a_1 \to gg$ and $a_1 \to c\bar{c}$ modes (in that order). For cases where the a_1 is approaching $2m_\tau$, $B(a_1 \to \tau^+\tau^-)$ declines, but is always bigger than 0.5 if $m_{a_1} > 2m_\tau$ with the residual mainly taken up by $B(a_1 \to c\bar{c})$. For the few $m_{a_1} < 2m_c$ points, $a_1 \to s\bar{s}$ is dominant.

As noted earlier, an important constraint on scenarios

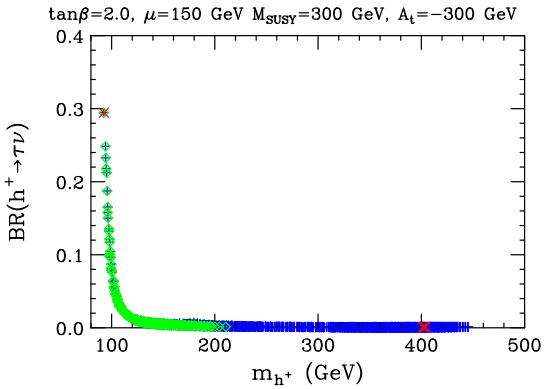

FIG. 13: $B(h^+ \to \tau^+ \nu_\tau)$ is plotted vs. m_{h^+} for the $\tan\beta = 2$, $m_{\rm SUSY} = 300$ GeV, $A = -300$ GeV scenario.

with a light a_1 is the branching ratio $B(\Upsilon \to \gamma a_1)$ which is strongly constrained by data from CLEO-III [20] for $m_{a_1} > 2m_\tau$. In particular, depending upon the precise value of m_{a_1} in the range between $2m_\tau$ and 7.5 GeV, the 95% CL upper limit on $B(\Upsilon \to \gamma a_1)$ is between 6×10^{-5} and 1.2×10^{-5}. In Fig. 18 we plot $B(\Upsilon \to \gamma a_1)$ as a

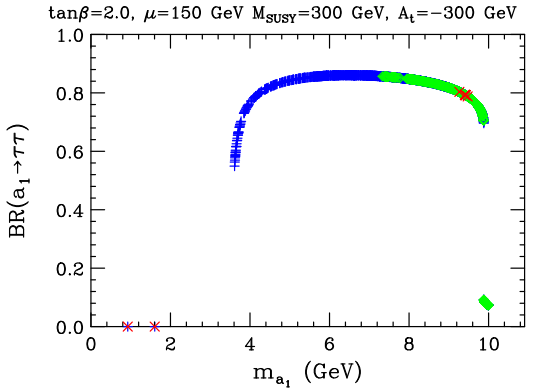

FIG. 14: $B(a_1 \to \tau^+\tau^-)$ is plotted vs. m_{a_1} for the $\tan\beta = 2$, $m_{\rm SUSY} = 300$ GeV, $A = -300$ GeV scenario.

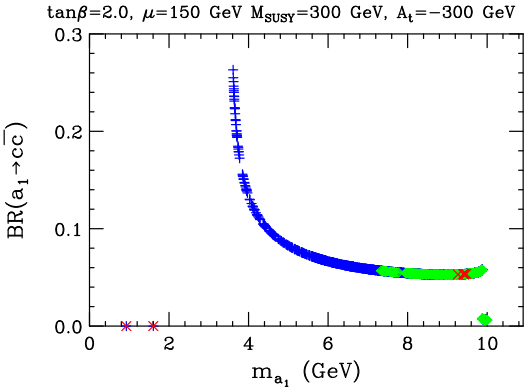

FIG. 15: $B(a_1 \to c\bar{c})$ is plotted vs. m_{a_1} for the $\tan\beta = 2$, $m_{\rm SUSY} = 300$ GeV, $A = -300$ GeV scenario.

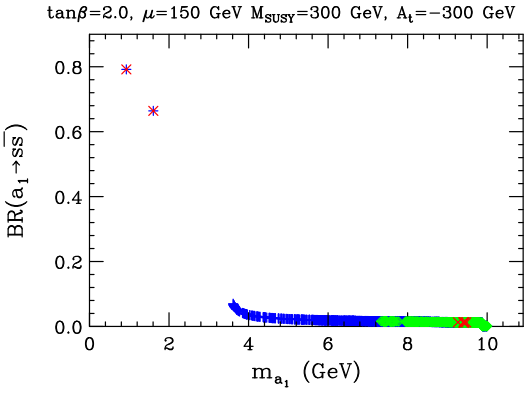

FIG. 16: $B(a_1 \to s\bar{s})$ is plotted vs. m_{a_1} for the $\tan\beta = 2$, $m_{\rm SUSY} = 300$ GeV, $A = -300$ GeV scenario.

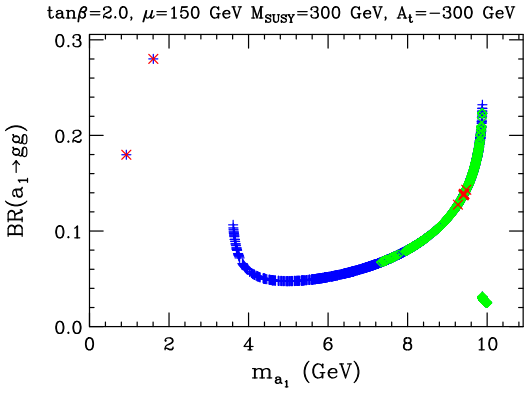

FIG. 17: $B(a_1 \to gg)$ is plotted vs. m_{a_1} for the $\tan\beta = 2$, $m_{\rm SUSY} = 300$ GeV, $A = -300$ GeV scenario.

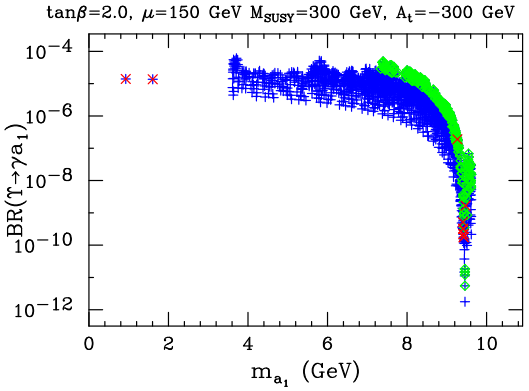

FIG. 18: $B(\Upsilon \to \gamma a_1)$ is plotted vs. m_{a_1} for the $\tan\beta = 2$, $m_{\rm SUSY} = 300$ GeV, $A = -300$ GeV scenario.

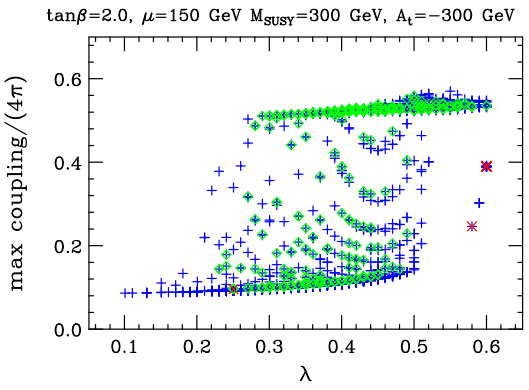

FIG. 19: $y_{\rm max}$ is plotted vs. λ for the $\tan\beta = 2$, $m_{\rm SUSY} = 300$ GeV, $A = -300$ GeV scenario.

function of m_{a_1} after imposing $B(\Upsilon \to \gamma a_1)$ constraints. We see that points with $\cos^2\theta_A > 0.5$ (the green diamonds) are only allowed at relatively large m_{a_1} and that even some points with $\cos^2\theta_A < 0.5$ have been eliminated in the $2m_\tau < m_{a_1} < 7.5$ GeV range. Thus, it is the $\Upsilon \to \gamma a_1 \to \gamma\tau^+\tau^-$ decay limits that rule out a_1-doublet-like scenarios with $m_{a_1} \lesssim 7.5$ GeV. The underlying reason for the a_1-doublet-like points to be more strongly excluded by Υ decays is that, as discussed earlier, the $a_1 b\bar{b}$ coupling is given by $C_{a_1 b\bar{b}} = \cos\theta_A \tan\beta$, which is, of course, largest for large $|\cos\theta_A|$.

Let us turn for a moment to a discussion of whether or not these scenarios are perturbative after evolution to the GUT scale. [3] The couplings of interest are λ, κ, h_t and h_b. At low $\tan\beta$, h_b always remains perturbative but λ, κ and h_t can become large. In Fig. 19 we plot the

[3] For small $\tan\beta$ the the top Yukawa coupling becomes non-perturbative close to the grand unification (GUT) scale. The exact value of $\tan\beta$ consistent with perturbativity all the way to the GUT scale depends on superpartner masses through SUSY threshold corrections to the top Yukawa coupling, and in the NMSSM it is about $\tan\beta \gtrsim 1.6$. However, adding extra vector-like complete SU(5) matter multiplets at the TeV scale, *e.g.* the parts of the sector that mediate SUSY breaking (messengers) or are present for no particular reason, does not affect the unification of gauge couplings while it slows down the running of the top Yukawa coupling [16, 17] and even $\tan\beta \simeq 1$ can be consistent with perturbative unification of gauge couplings.

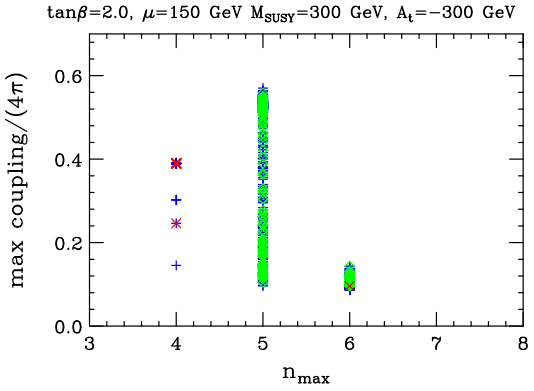

FIG. 20: $y_{\rm max}$ is plotted vs. $n_{\rm max}$ for the $\tan\beta = 2$, $m_{\rm SUSY} = 300$ GeV, $A = -300$ GeV scenario.

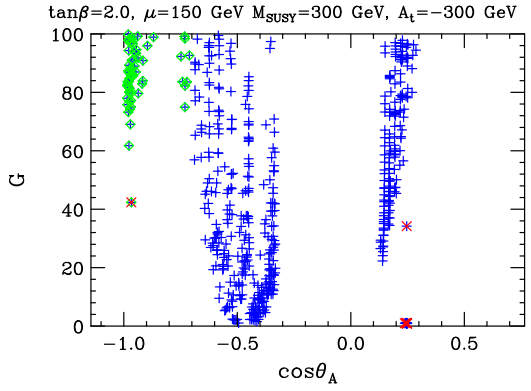

FIG. 21: G is plotted vs. $\cos\theta_A$ for the $\tan\beta = 2$, $m_{\rm SUSY} = 300$ GeV, $A = -300$ GeV scenario. The displayed points comprise only a small fraction of the total number of points appearing in previous figures.

value of

$$y_{\rm max} \equiv \frac{\max\{\lambda, \kappa, h_t, h_b\}}{4\pi} \tag{7}$$

at the GUT scale as a function of λ for the various scenarios in our $\tan\beta = 2$ scan. A value of $y_{\rm max} = 0.5$ indicates that the evolution has gone non perturbative. In Fig. 20, we show which of the couplings is largest or has gone non-perturbative first using the code $4 \equiv \lambda$, $5 \equiv \kappa$, $6 \equiv h_t$ and $7 \equiv h_b$. We observe that it is most often κ that has the largest coupling at the GUT scale, especially for the $\cos^2\theta_A > 0.5$ scenarios.

Another issue of interest is whether finetuning of the NMSSM parameters (in particular A_λ and A_κ) is required (either at scale m_Z or at the GUT scale) in order to obtain $m_{a_1} < 10$ GeV and scenarios that escape LEP and other limits. In [9] we developed a measure G of this fine tuning. In Fig. 21, we plot G as a function of $\cos\theta_A$. We see that small values of G arise for quite specific values of $\cos\theta_A$, namely $-0.6 \lesssim \cos\theta_A \lesssim -0.4$ and $0.15 \lesssim \cos\theta_A \lesssim 0.22$. Note that the a_1-doublet-like scenarios typically have moderately large G values — only if the a_1 is singlet like is it possible for there to be no need for tuning A_λ and A_κ in order to achieve $m_{a_1} < 2m_b$ *and* large $B(h_1 \to a_1 a_1)$ (to escape LEP limits) simultaneously.

In our scans, we did not specifically exclude scenarios because of difficulties with precision electroweak constraints (mainly the parameter T) or the anomalous magnetic moment of the muon, a_μ. In fact, for all the points plotted, $-0.002 < \Delta T < 0.011$, where ΔT is defined relative to a SM-like Higgs with mass 100 GeV, and $-2.2 \times 10^{-10} < \delta a_\mu < -1.4 \times 10^{-10}$ where δa_μ is the net contribution of the entire Higgs sector. Clearly, the size of ΔT is such that the Higgs sector of the NMSSM models being considered makes a very small contribution to T while δa_μ is also so small as to have little impact on the current discrepancy between the SM prediction for a_μ and the experimental observation, which difference is of order 30×10^{-10}.

Finally, we show in Figs. 22 and 23 the λ, κ, A_λ and

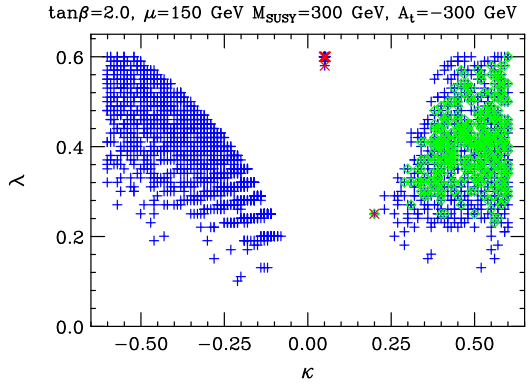

FIG. 22: λ is plotted vs. κ for the $\tan\beta = 2$, $m_{\rm SUSY} = 300$ GeV, $A = -300$ GeV scenario.

A_κ values which yield the points plotted in the preceding figures. The main observation is that the $\cos^2\theta_A > 0.5$ points require $\kappa > 0$ and $A_\kappa, A_\lambda < 0$. Note also the small number of points with κ close to zero. Many, but not all, of the very small $m_{h_1} < 65$ GeV scenarios arise from these points.

B. Results for $\tan\beta = 1.7$

One can avoid non-perturbative couplings for a large number of allowed points for lower $\tan\beta$ if $m_{\rm SUSY}$ and A_t are somewhat larger. As an example, we present results for the case of $\tan\beta = 1.7$, $m_{\rm SUSY} = 500$ GeV and $A = -1000$ GeV in Figs. 24-42. The point notation is as for $\tan\beta = 2$, except that in this case there are points for which $B(h_1 \to a_1 a_1) < 0.7$. These points are indicated by the yellow squares.

As in the previous case, significant restrictions are placed on $|\cos\theta_A|$ due to limits on the $C_{a_1 b\bar{b}}$ coupling. Fig. 24 shows that once again these restrictions basically imply a limit on $\cos^2\theta_A$ that is significantly below 0.5 if

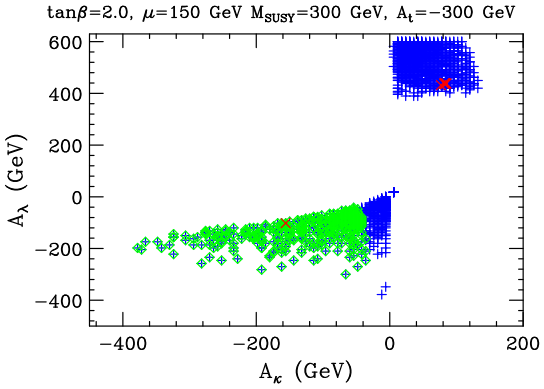

FIG. 23: A_λ is plotted vs. A_κ for the $\tan\beta = 2$, $m_{\rm SUSY} = 300$ GeV, $A = -300$ GeV scenario.

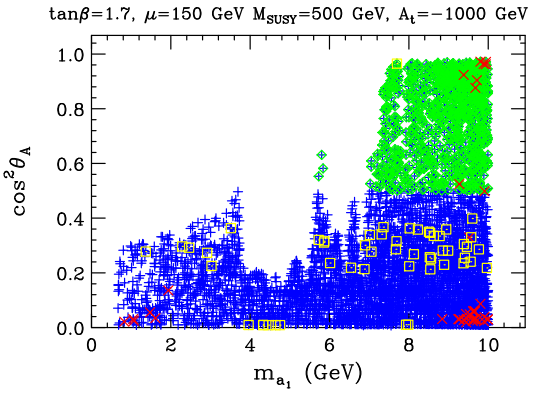

FIG. 24: $\cos^2\theta_A$ is plotted vs. m_{a_1} for the $\tan\beta = 1.7$, $m_{\rm SUSY} = 500$ GeV, $A = -1000$ GeV scenario.

$m_{a_1} \lesssim 7.5$ GeV.

We now repeat the same set of figures as in the $\tan\beta = 2$ case. Many of the same comments apply. Where appropriate we shall comment on differences.

We note that we have found many more points with quite low m_{h_1} for this case as compared to the $\tan\beta = 2$

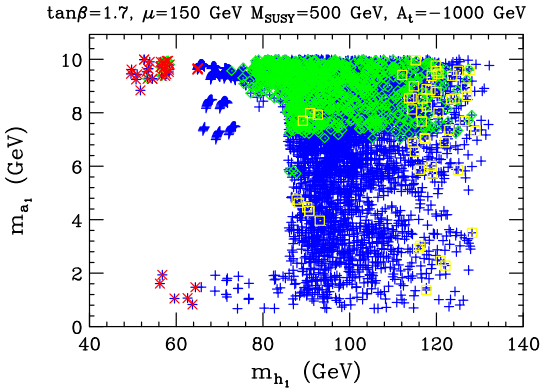

FIG. 25: m_{a_1} is plotted vs. m_{h_1} for the $\tan\beta = 1.7$, $m_{\rm SUSY} = 500$ GeV, $A = -1000$ GeV scenario.

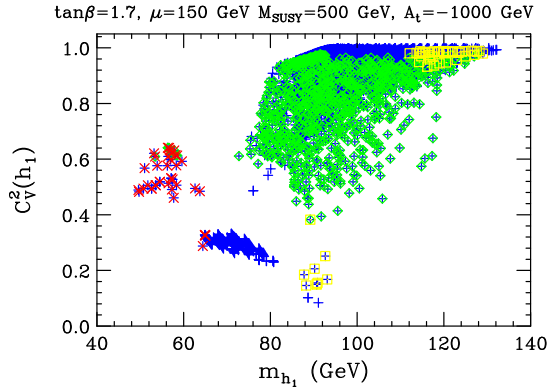

FIG. 26: $C_V^2(h_1)$ is plotted vs. m_{h_1} for the $\tan\beta = 1.7$, $m_{\rm SUSY} = 500$ GeV, $A = -1000$ GeV scenario.

TABLE I: Selected points for which m_{h_1} and corresponding m_{h_2} lie within the LEP excess region and the corresponding $C_V^2(h_1)B(h_1 \to b\bar{b})$ and $C_V^2(h_2)B(h_2 \to b\bar{b})$ values.

m_{h_1}	$C_V^2(h_1)B(h_1 \to b\bar{b})$	m_{h_2}	$C_V^2(h_2)B(h_2 \to b\bar{b})$
93.1	0.0684	96.2	0.1590
90.7	0.0560	96.6	0.1726
90.2	0.1171	97.2	0.1468
88.3	0.0557	97.0	0.1803
87.8	0.0974	97.5	0.1609
90.7	0.0560	96.6	0.1727
92.7	0.1748	97.2	0.1037
90.9	0.0599	97.1	0.1416

scenario previously considered. Of particular interest is the fact that there are a significant number of model points for which m_{h_1} is near 90 GeV and m_{h_2} is just below 100 GeV with $C_V^2(h_1)B(h_1 \to b\bar{b}) \sim 0.1 - 0.2$ and $C_V^2(h_2)B(h_2 \to b\bar{b}) \sim 0.1 - 0.2$. A particular subset of these can be identified in Figs. 28 and 33 as the yellow squares with the above attributes. (However, there are quite a few blue points that also satisfy these criteria.) The precise masses and $C_V^2 B(h \to b\bar{b})$ values of the yellow-square points are tabulated in Table II B. These points appear in Fig. 24 as the yellow squares with $\cos^2\theta_A \sim 0$ (more precisely $\cos\theta_A \sim 0.1$) and $m_{a_1} \sim 4$ GeV or 8 GeV. They appear in Figs. 41 and 42 as the yellow square points with $\kappa \in [-0.046, -0.041]$, $\lambda \sim 0.14 - 0.15$, $A_\kappa \sim 6 - 7$ GeV and $A_\lambda \sim 486 - 492$ GeV. The $\cos\theta_A$, κ and A_κ values indicate that these points are ones that are close to the Peccei-Quinn symmetry limit of the NMSSM.

The reason that these points are of particular interest is that the two Higgs bosons combine to nicely explain the LEP excess seen throughout the entire $m_{b\bar{b}} \in [88\ {\rm GeV}, 100\ {\rm GeV}]$ mass region in the $e^+e^- \to Zb\bar{b}$ channel. The level of this excess corresponds to $C_V^2 B(h \to b\bar{b}) \sim 0.1 - 0.2$ for any single h mass in this region. The masses of the two Higgs bosons are typically separated

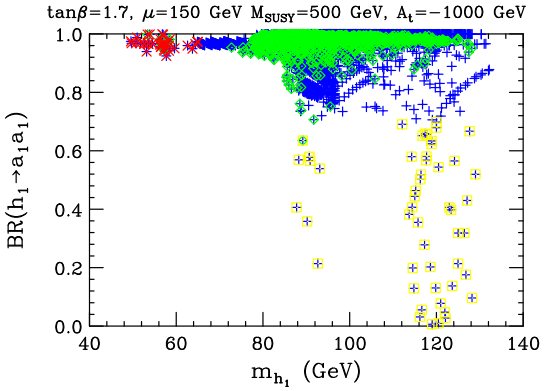

FIG. 27: $B(h_1 \to a_1 a_1)$ is plotted vs. m_{h_1} for the $\tan\beta = 1.7$, $m_{\rm SUSY} = 500$ GeV, $A = -1000$ GeV scenario.

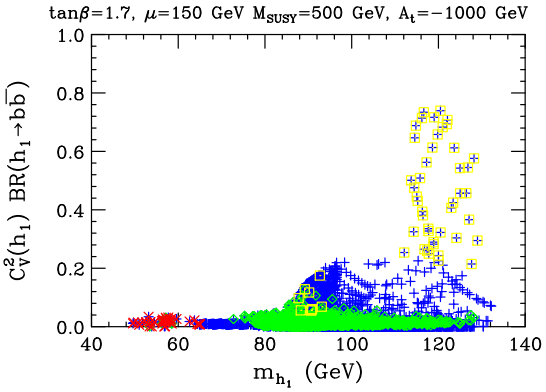

FIG. 28: $C_V^2(h_1)B(h_1 \to b\bar{b})$ is plotted vs. m_{h_1} for the $\tan\beta = 1.7$, $m_{\rm SUSY} = 500$ GeV, $A = -1000$ GeV scenario.

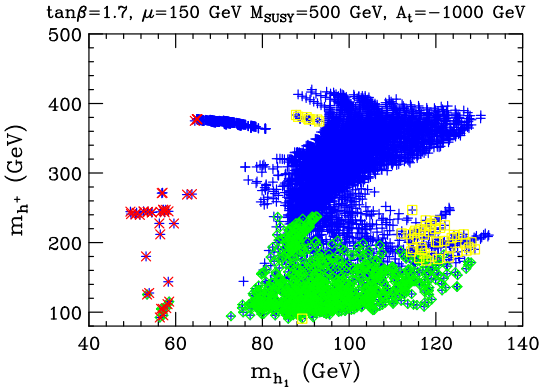

FIG. 29: m_{h^+} is plotted vs. m_{h_1} for the $\tan\beta = 1.7$, $m_{\rm SUSY} = 500$ GeV, $A = -1000$ GeV scenario.

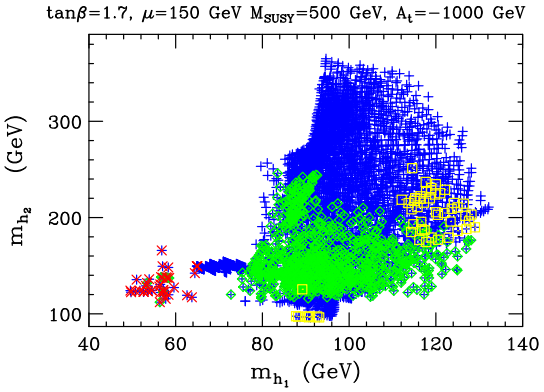

FIG. 30: m_{h_2} is plotted vs. m_{h_1} for the $\tan\beta = 1.7$, $m_{\rm SUSY} = 500$ GeV, $A = -1000$ GeV scenario.

by about $2\sigma_{res}$ where $\sigma_{res} \sim 3$ GeV was the LEP mass resolution. As a result, the combination of the two Higgses would give the broad excess observed. The manner in which $C_V^2 B(h \to b\bar{b}) \sim 0.1 - 0.2$ is achieved is quite different for h_1 vs. h_2. In the case of the h_1, $C_V^2(h_1)$ (see Fig. 26) is small and $B(h_1 \to b\bar{b})$ is fairly large (because $B(h_1 \to a_1 a_1)$ is relatively small (see Fig. 27). In the case of the h_2, $C_V^2(h_2)$ (see Fig. 31) is large and $B(h_2 \to b\bar{b})$ is fairly small (because $B(h_2 \to a_1 a_1)$ is relatively large (see Fig. 32).

These special points are also rather attractive in that they are ones for which the couplings remain perturbative after evolution evolution to the GUT scale (see the yellow-square points with small λ in Fig. 38). However, for these points the A_κ-A_λ fine-tuning measure G (see the yellow-square points in Fig. 40 with $\cos\theta_A \sim 0.1$) is somewhat large.

As regards the a_1-doublet-like (green diamond) points, we observe from Fig. 30 that the lower bound on m_{h_2} has been pushed to about 110 GeV vs. the ~ 100 GeV value obtained for $\tan\beta = 2$. This means that Zh_2 production at LEP would have been minimal or absent for such cases, but there would still have been a significant rate for $h_2 a_1$ production. However, to repeat, LEP did not look for the relevant $h_2 a_1 \to a_1 a_1 a_1$ or $h_2 a_1 \to Z a_1 a_1$ final states that would have been dominant (Figs. 32 and 34, respectively).

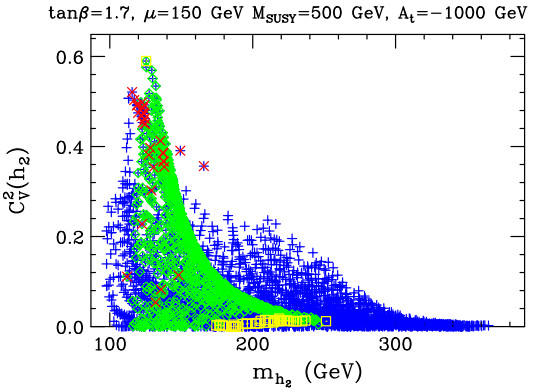

FIG. 31: $C_V^2(h_2)$ is plotted vs. m_{h_2} for the $\tan\beta = 1.7$, $m_{\rm SUSY} = 500$ GeV, $A = -1000$ GeV scenario.

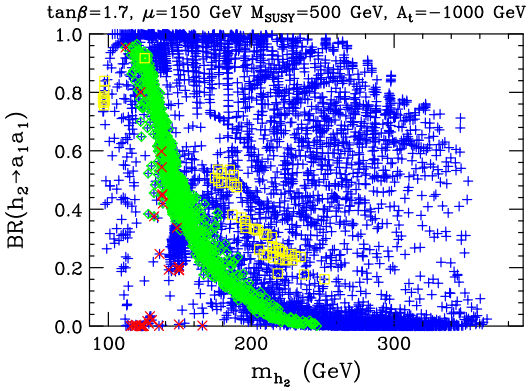

FIG. 32: $B(h_2 \to a_1 a_1)$ is plotted vs. m_{h_2} for the $\tan\beta = 1.7$, $m_{\rm SUSY} = 500$ GeV, $A = -1000$ GeV scenario.

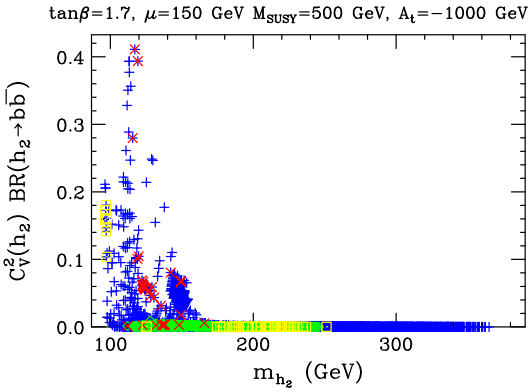

FIG. 33: $C_V^2(h_2) B(h_2 \to b\bar{b})$ is plotted vs. m_{h_2} for the $\tan\beta = 1.7$, $m_{\rm SUSY} = 500$ GeV, $A = -1000$ GeV scenario.

C. Results for $\tan\beta = 1.2$

We have also performed a scan for the case of $\tan\beta = 1.2$, $m_{\rm SUSY} = 500$ GeV and $A = -1000$ GeV. For the most part, results are very similar to those for $\tan\beta = 1.7$, $m_{\rm SUSY} = 500$ GeV and $A = -1000$ GeV. One difference arises because the coupling of the a_1 to $b\bar{b}$, proportional to $\cos\theta_A \tan\beta$ is weaker for the lower $\tan\beta$ value. This implies that the experimental upper limits on this coupling are less restrictive at a given value of $\cos\theta_A$. The result is that $|\cos\theta_A|^2 > 0.5$ is possible for $m_{a_1} < 2m_\tau$ (*i.e.* below the m_{a_1} values for which

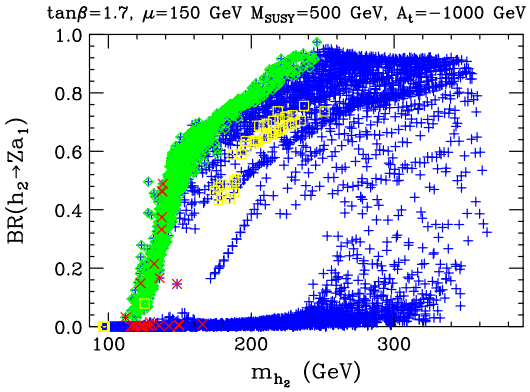

FIG. 34: $B(h_2 \to Z a_1)$ is plotted vs. m_{h_2} for the $\tan\beta = 1.7$, $m_{\rm SUSY} = 500$ GeV, $A = -1000$ GeV scenario.

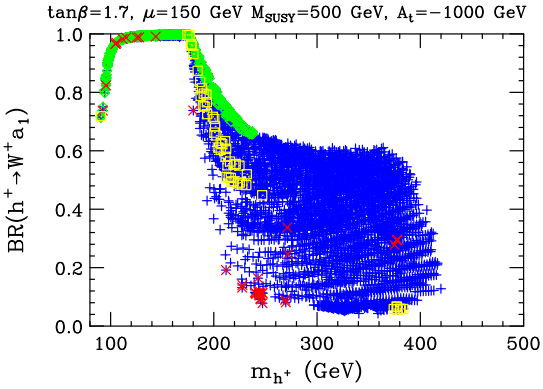

FIG. 35: $B(h^+ \to W^{+(\star)} a_1)$ is plotted vs. m_{h^+} for the $\tan\beta = 1.7$, $m_{\rm SUSY} = 500$ GeV, $A = -1000$ GeV scenario.

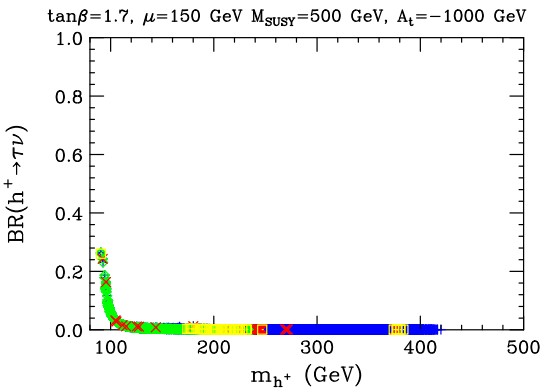

FIG. 36: $B(h^+ \to \tau^+ \nu_\tau)$ is plotted vs. m_{h^+} for the $\tan\beta = 1.7$, $m_{\rm SUSY} = 500$ GeV, $A = -1000$ GeV scenario.

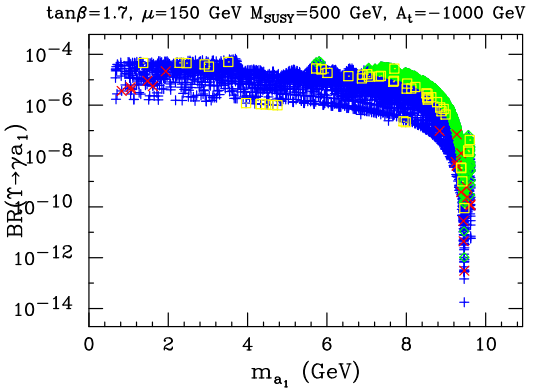

FIG. 37: $B(\Upsilon \to \gamma a_1)$ is plotted vs. m_{a_1} for the $\tan\beta = 1.7$, $m_{\rm SUSY} = 500$ GeV, $A = -1000$ GeV scenario.

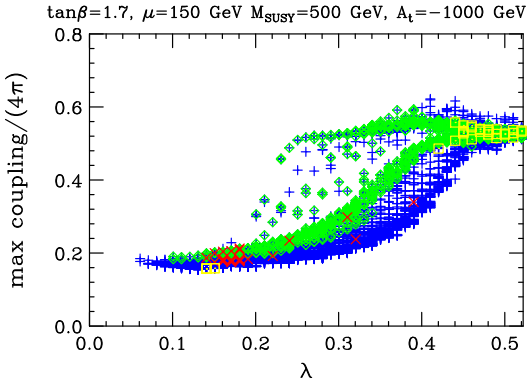

FIG. 38: $y_{\max}$ is plotted vs. λ for the $\tan\beta = 1.7$, $m_{\rm SUSY} = 500$ GeV, $A = -1000$ GeV scenario.

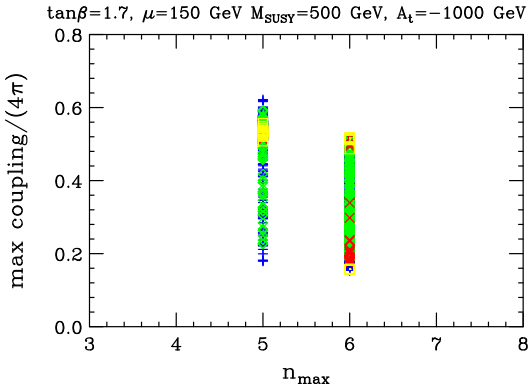

FIG. 39: $y_{\max}$ is plotted vs. $n_{\max}$ for the $\tan\beta = 1.7$, $m_{\rm SUSY} = 500$ GeV, $A = -1000$ GeV scenario.

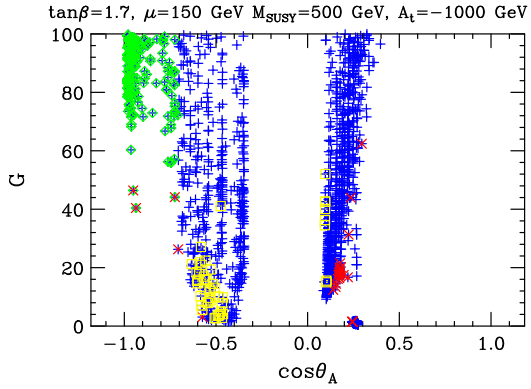

FIG. 40: G is plotted vs. $\cos\theta_A$ for the $\tan\beta = 1.7$, $m_{\rm SUSY} = 500$ GeV, $A = -1000$ GeV scenario. The displayed points comprise only a small fraction of the total number of points appearing in previous figures.

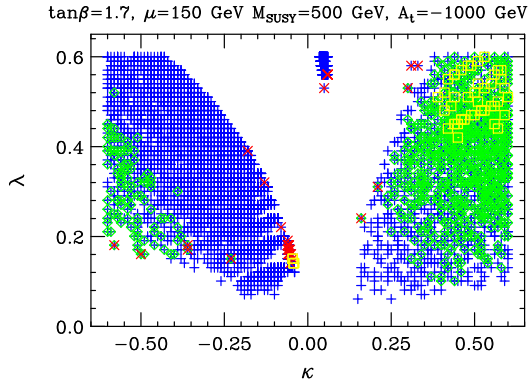

FIG. 41: λ is plotted vs. κ for the $\tan\beta = 1.7$, $m_{\rm SUSY} = 500$ GeV, $A = -1000$ GeV scenario.

the $a_1 b\bar{b}$ coupling is so strongly limited by CLEO-III results). This is made apparent by comparing Fig. 43 to Fig. 24. Another difference is that for all but a special class (to be described later) of the $\tan\beta = 1.2$ scenarios, one or more of the couplings, λ, κ, A_λ or A_κ becomes non-perturbative in evolving to the GUT scale.

In Fig. 44 we plot m_{h^+} vs. m_{h_1}. We see that the lowest value of m_{h^+} is about 90 GeV and arises for the a_1-doublet-like scenarios. There are a significant number of points with $m_{h_1} < 65$ GeV, all of which have a very singlet-like a_1, as is most apparent from the red crosses in Fig. 43. Fig. 45 shows m_{h_2} vs. m_{h_1}. We see that m_{h_2} values as low as 90 GeV are possible for singlet-like a_1, whereas the lower limit on m_{h_2} for a_1-doublet-like scenarios has risen to about 140 GeV as compared to the lower values found for $\tan\beta = 1.7$ and 2.

For this $\tan\beta = 1.2$ case, there are many points with m_{h_2} in the $95 - 100$ GeV interval and m_{h_1} in the $90 - 96$ GeV interval with both $C_V^2(h_1)B(h_1 \to b\bar{b})$ and $C_V^2(h_2)B(h_2 \to b\bar{b})$ between 0.05 and 0.15 that would explain the broad excess in this region seen at LEP. As for $\tan\beta = 1.7$, all these points have very small κ and A_κ and are therefore close to the PQ symmetry limit of the model. Most of these points are such that the couplings do not quite reach the non-perturbative value of coupling/$(4\pi) = 0.5$ at the GUT scale. Rather coupling/$(4\pi) \sim 0.4$ is a typical maximum value. In this sense they are the most attractive of the $\tan\beta = 1.2$ scenarios. As for the blue points of this type in the $\tan\beta = 1.7$ case, the points in this special class at $\tan\beta = 1.2$ typically also have very modest A_λ, A_κ finetuning measure G, with G values between 10 and 30 being typical. One point of difference with $\tan\beta = 1.7$ is that the $\tan\beta = 1.2$ special points all have $B(h_1 \to a_1 a_1) > 0.75$.

For this smaller $\tan\beta = 1.2$ value, $B(t \to h^+ b)$ is larger (~ 0.3) at the lowest $m_{h^+} \sim 90$ GeV mass than for $\tan\beta = 1.7$. Nonetheless, the Tevatron is still unable to limit these scenarios since $B(h^+ \to \tau^+\nu_\tau) < 0.2$ (see Fig. 46) given the dominance of $h^+ \to W^{+(\star)} b$ decays (Fig. 47).

III. CONCLUSIONS

For low $\tan\beta$ values in the NMSSM, we have found many interesting new Higgs scenarios with a light CP-

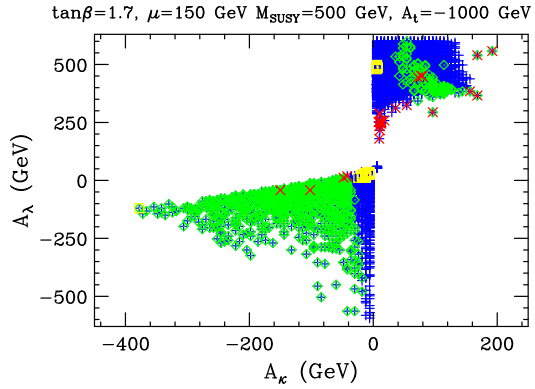

FIG. 42: A_λ is plotted vs. A_κ for the $\tan\beta = 1.7$, $m_{\rm SUSY} = 500$ GeV, $A = -1000$ GeV scenario.

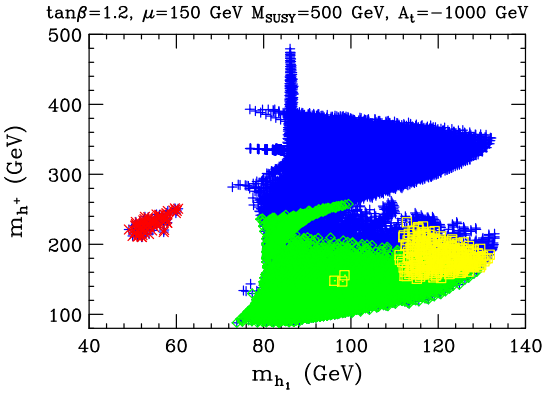

FIG. 44: m_{h^+} is plotted vs. m_{h_1} for the $\tan\beta = 1.2$, $m_{\rm SUSY} = 500$ GeV, $A = -1000$ GeV scenario.

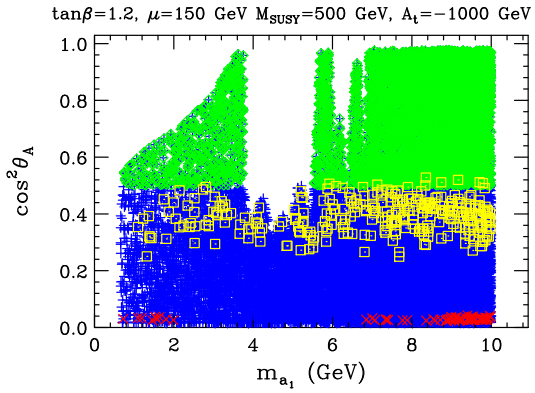

FIG. 43: $\cos^2\theta_A$ is plotted vs. m_{a_1} for the $\tan\beta = 1.2$, $m_{\rm SUSY} = 500$ GeV, $A = -1000$ GeV scenario.

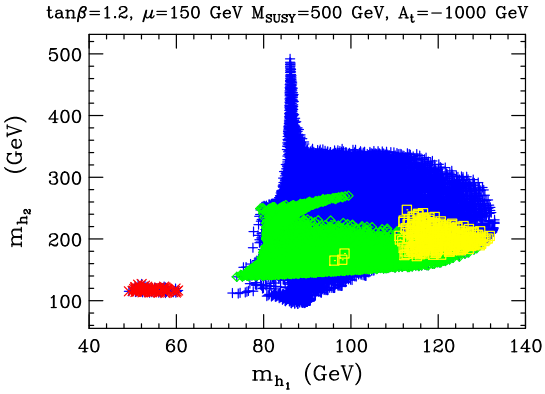

FIG. 45: m_{h_2} is plotted vs. m_{h_1} for the $\tan\beta = 1.2$, $m_{\rm SUSY} = 500$ GeV, $A = -1000$ GeV scenario.

odd scalar with mass below 10 GeV. For many of the experimentally allowed parameter choices, the h_1, h^+ and h_2 are all sufficiently light as to be kinematically accessible at LEP and the Tevatron, but they decay into final states containing the light CP-odd scalar and therefore escaped detection. One particularly interesting parameter space region is that associated with the PQ symmetry limit (small $|\kappa|$ and small A_κ) in which the h_1 has mass near 90 GeV and the h_2 has mass near 100 GeV (*i.e.* basically non-overlapping within experimental resolution) and $g^2_{ZZh_1}B(h_1 \to b\overline{b})$ and $g^2_{ZZh_2}B(h_2 \to b\overline{b})$ are such as to explain the observed LEP excess throughout this region. These points, such that both h_1 and h_2 contribute to the LEP excess, are present for the $\tan\beta = 1.2$ and $\tan\beta = 1.7$ cases, but not for $\tan\beta = 2$.

Another important common feature of all these low-$\tan\beta$ scenarios that is also shared with the high-$\tan\beta$ scenarios explored in earlier papers is that for any given m_{a_1} there is always a lower limit on $B(\Upsilon \to \gamma a_1)$. This lower limit is above about 5×10^{-7} for $m_{a_1} < 7.5$ GeV. We are hopeful that this is a level that can eventually be probed by BaBar and Belle. This lower limit arises because there is a lower limit on $|\cos\theta_A|$, and therefore on $C_{a_1 b\overline{b}} = \cos\theta_A \tan\beta$, below which $B(h_1 \to a_1 a_1)$ is not large enough for a light h_1 to have escaped LEP limits.

We should further comment that all the scenarios of the present paper, as well as previous papers that focused on higher-$\tan\beta$, are such that the scenarios that survive all experimental constraints are ones for which the contributions of the Higgs sector to both the precision electroweak observables, ΔT and ΔS (relative to the SM-Higgs contribution for $m_{h_{\rm SM}} = 110$ GeV), and to the muon anomalous magnetic moment, a_μ (relative to the observed experimental discrepancy) are very small. In the case of ΔT and ΔS the small extra ΔT can be understood as a natural result of either h_3 and a_2 decoupling or of h_2 and a_2 decoupling.

Overall, the NMSSM provides a huge opportunity to have an "Ideal Higgs" boson scenario in which there is one or two light Higgs bosons (masses at or below 100 GeV) that in combination have all the ZZ-Higgs coupling squared and therefore give values for the precision

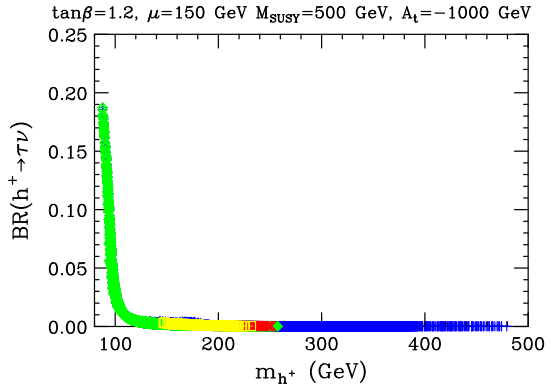

FIG. 46: $B(h^+ \to W^{+(\star)} a_1)$ is plotted vs. m_{h^+} for the $\tan\beta = 1.2$, $m_{\rm SUSY} = 500$ GeV, $A = -1000$ GeV scenario.

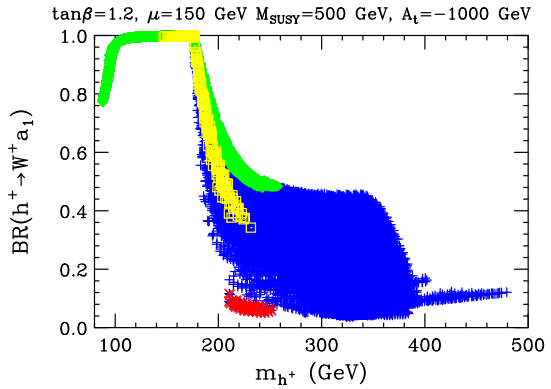

FIG. 47: $B(h^+ \to W^{+(\star)} a_1)$ is plotted vs. m_{h^+} for the $\tan\beta = 1.2$, $m_{\rm SUSY} = 500$ GeV, $A = -1000$ GeV scenario.

electroweak observables S and T that are in excellent agreement with data. These Higgs bosons escape LEP limits because of unusual decays involving the light a_1 with $m_{a_1} < 2m_b$ that is the common future of all these "Ideal" models. They also provide an excellent possibility for describing the broad excess in the $e^+e^- \to Zb\overline{b}$ channel in the region $m_{b\overline{b}} \in [90\ {\rm GeV}, 105\ {\rm GeV}]$ seen at LEP. We look forward to possibly discovering the a_1 in Υ decays at Babar or Belle, or direct detection of $h_1 \to a_1 a_1$ at the LHC, if not the Tevatron.

Acknowledgments

We would like to thank A. Akeroyd and Ricardo Eusebi for discussions. JFG is supported by U.S. Department of Energy grant DE-FG02-91ER40674. JFG would like to thank the Aspen Center for Physics and KITP at U.C. Santa Barbara for support and hospitality during various phases of this work. The part of this research performed at KITP was supported by the National Science Foundation under Grant No. PHY05-51164.

[1] For a review and references, see, S. Chang, R. Dermisek, J. F. Gunion and N. Weiner, arXiv:0801.4554 [hep-ph].
[2] R. Dermisek, arXiv:0806.0847 [hep-ph].
[3] G. Abbiendi *et al.* [OPAL Collaboration], Eur. Phys. J. C **27**, 311 (2003) [arXiv:hep-ex/0206022].
[4] LEP Collaborations, arXiv:hep-ex/0412015.
[5] R. Dermisek, arXiv:0807.2135 [hep-ph].
[6] J. R. Ellis, J. F. Gunion, H. E. Haber, L. Roszkowski and F. Zwirner, Phys. Rev. D **39**, 844 (1989).
[7] R. Dermisek and J. F. Gunion, Phys. Rev. Lett. **95**, 041801 (2005) [arXiv:hep-ph/0502105].
[8] R. Dermisek and J. F. Gunion, Phys. Rev. D **73**, 111701 (2006) [arXiv:hep-ph/0510322].
[9] R. Dermisek and J. F. Gunion, Phys. Rev. D **75**, 075019 (2007) [arXiv:hep-ph/0611142].
[10] R. Dermisek and J. F. Gunion, Phys. Rev. D **76**, 095006 (2007) [arXiv:0705.4387 [hep-ph]].
[11] R. Dermisek, J. F. Gunion and B. McElrath, Phys. Rev. D **76**, 051105 (2007) [arXiv:hep-ph/0612031].
[12] See, e.g. V. Barger, P. Langacker, H. S. Lee and G. Shaughnessy, Phys. Rev. D **73**, 115010 (2006);
[13] R. Dermisek and J. F. Gunion, Phys. Rev. D **77**, 015013 (2008) [arXiv:0709.2269 [hep-ph]].
[14] H. P. Nilles, M. Srednicki and D. Wyler, Phys. Lett. B **120** (1983) 346. J. M. Frere, D. R. T. Jones and S. Raby, Nucl. Phys. B **222** (1983) 11. J. P. Derendinger and C. A. Savoy, Nucl. Phys. B **237** (1984) 307. J. R. Ellis, J. F. Gunion, H. E. Haber, L. Roszkowski and F. Zwirner, Phys. Rev. D **39** (1989) 844. M. Drees, Int. J. Mod. Phys. A **4** (1989) 3635. U. Ellwanger, M. Rausch de Traubenberg and C. A. Savoy, Phys. Lett. B **315** (1993) 331 [arXiv:hep-ph/9307322], and Nucl. Phys. B **492** (1997) 21 [arXiv:hep-ph/9611251], S. F. King and P. L. White, Phys. Rev. D **52** (1995) 4183 [arXiv:hep-ph/9505326]. F. Franke and H. Fraas, Int. J. Mod. Phys. A **12** (1997) 479 [arXiv:hep-ph/9512366].
[15] U. Ellwanger, J. F. Gunion and C. Hugonie, arXiv:hep-ph/0406215.
[16] M. Masip, R. Munoz-Tapia and A. Pomarol, Phys. Rev. D **57**, 5340 (1998) [arXiv:hep-ph/9801437].
[17] R. Barbieri, L. J. Hall, A. Y. Papaioannou, D. Pappadopulo and V. S. Rychkov, JHEP **0803**, 005 (2008).

[18] S. Schael *et al.* [LEP Collaborations], Eur. Phys. J. C **47**, 547 (2006) [arXiv:hep-ex/0602042].
[19] M. A. Sanchis-Lozano, Mod. Phys. Lett. A **17**, 2265 (2002); Int. J. Mod. Phys. A **19**, 2183 (2004); E. Fullana and M. A. Sanchis-Lozano, Phys. Lett. B **653**, 67 (2007).
[20] W. Love, *et al.*(CLEO), CLNS 08/2033, CLEO 08-16 to be submitted to PRL.
[21] J. Lee-Franzini, Eloisatron Workshop: Higgs 1989:0269-294 (QCD161:I12:1989).
[22] G. Abbiendi *et al.* [OPAL Collaboration], Eur. Phys. J. C **23**, 397 (2002) [arXiv:hep-ex/0111010].
[23] The Delphi Collaboration, ICHEP 2002, DELPHI 2002-037-CONF-571. I employ Table 20 — these are very close to those appearing in the figures of J. Abdallah *et al.* [DELPHI Collaboration], Eur. Phys. J. C **38**, 1 (2004) [arXiv:hep-ex/0410017].
[24] J. F. Gunion, arXiv:0808.2509 [hep-ph].
[25] R. Dermisek and J.F. Gunion, in preparation.
[26] [LEP Higgs Working Group for Higgs boson searches and ALEPH Collaboration an], arXiv:hep-ex/0107031.
[27] J. Abdallah *et al.* [DELPHI Collaboration], Eur. Phys. J. C **34**, 399 (2004) [arXiv:hep-ex/0404012].
[28] G. Grenier, arXiv:0710.0853 [hep-ex].
[29] CDF Collaboration, CDF Note 9322, 2008, preliminary results.
[30] D0 Collaboration, D0 Note 4715-CONF, 2008, preliminary results.
[31] A. G. Akeroyd, A. Arhrib and Q. S. Yan, Eur. Phys. J. C **55**, 653 (2008) [arXiv:0712.3933 [hep-ph]].